Wear load analysis of conical cutter crushing rock based on SPH to SPH interaction method

Indexed by:
Web of Science Group

Xiaohui Liu[a], Junwei Zhai[a,*], Lei Guo[a], Leilei Cao[b,a], Penghui Wang[a]

a Key Laboratory of Road Construction Technology and Equipment of MOE, Chang'an University, China
b Guangxi Key Laboratory of Manufacturing System & Advanced Manufacturing Technology, Guangxi University, China

Highlights

- A dynamic model for cutter crushing rock is established using SPH-SPH interaction method

- The relationship between the wear and cutting performance factors was analyzed.

- The cutting angle selection reference was given under different consideration factors.

Abstract

Wear is the main failure type for conical cutters. The main load causing its wear is difficult to measure in the test, and the existing simulation models cannot simulate the wear load. Thus, the three-dimensional dynamic model for conical cutter crushing rock is established based on the SPH-SPH interaction method to analyze the relationship between the cutting performance factors and cutter wear. The factors are taken into account such as the stress distribution of rock, kinetic energy and internal energy and displacement of rock, cutting load of cutter, stress of cutter. Then, it is studied that the effect of cutting angle on the cutting performance parameters such as specific energy consumption, rock avalanching, cutting load, load fluctuation, cutter tip stress and cutter side stress. Finally, the cutting angle selection reference of the cutter is given under different consideration factors.

Keywords
rock breaking, SPH, dynamic model, conical cutter, wear

1. Introduction

Conical cutters are the main tools used for rock crushing, which are mainly used for coal mining, tunnels and other projects, shown in Fig.1(a). Many scholars at home and abroad have paid attention to the failure research of conical cutters [1-2], and pointed out that its failure types mainly include premature wear, carbide tip shedding, tool chipping, tool fracture and normal wear. And the proportion of different tool failure types shown in Fig.1(b), the failures caused by wear, such as normal wear, premature wear and carbide tip shedding, account for 75% of the total failure types.

As we all know, the failure of a conical cutter is directly related to the load it receives. Therefore, domestic and foreign scholars have long devoted themselves to the research of load on conical cutters used theory, experiment and simulation methods. In theory, Evans [3] first proposed a theoretical model for predicting the cutting force of conical cutters. Afterwards, Roxborough and Liu [4], Goktan [5-6], and Bilgin [7] made effective improvements to the Evans model, or used experimental fitting methods to improve the theoretical model. Until the past three years, there were still scholars carrying out the prediction research of the cutting force of conical cutters [8-10], and used it to calculate the cutting specific energy

(*) Corresponding author.
E-mail addresses: 2093551648@qq.com

X. Liu (ORCID: 0000-0003-4951-9041) chd160039@chd.edu.cn, J. Zhai (ORCID: 0009-0007-1619-0637) 2093551648@qq.com, L. Guo (ORCID: 0000-0002-5063-5296) lguo@chd.edu.cn, L. Cao (ORCID: 0000-0003-0384-1983) caoleilei@chd.edu.cn, P. Wang (ORCID: 0000-0003-3776-8577) wangpenghui@chd.edu.cn

consumption [11-12]. However, these theoretical models ignored the normal force and lateral force, and almost cannot be used to study the wear of cutters.

In terms of experiments, scholars have built different single conical cutter test devices, such as full-scale cutting rig [6-7], Automated Rotary Coal/rock Cutting Simulator (ARCCS) [13-14], and coal and rock cutting test bed [15-16], single-tooth cutting system [17-19], Vertical rock cutting rig (VRCR) [20], Coal-Rock

Cutting Machine (CCM) [21] and modified test devices [22-25], etc. Similar to theoretical research, the cutting force can only explain the load condition of the cutter and calculate the specific energy consumption to a certain extent, but it cannot analyze the wear of the cutter. Therefore, if the wear of the cutter wants to be studied, the load condition in the normal and lateral directions must be considered.

(a) Projects of coal mining and tunnels

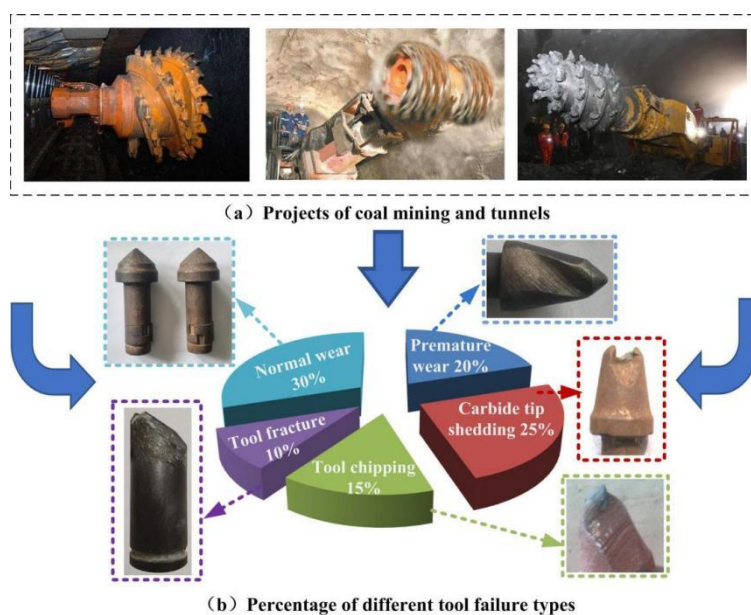(b) Percentage of different tool failure types

Fig.1. Application and failure types of conical cutter.

Zhang [26] and Fan [27-28] used the cutting force sensor to measure the three-directional load of the cutter, and analyzed the wear condition of the cutter. However, the accurate lateral force was not measured, and the specific part of the wear was not analyzed according to the three-directional load. Yang [29-30] directly used experiments to study the influence of cutter installation angle on cutter wear, but the normal force and lateral force of the cutter were not measured. Liu [31-32] controlled the influence factor of the cutter rotation, and directly studied the wear of the cutter by experiments. Although it has not measured the normal and the lateral force of the cutter, it pointed out that the wear mainly occurs on the back face of the cutter (Fig.6 in reference [32]) and used finite element simulation to analyze the cutter load distribution. Moreover, this inference can be verified by the test results of rock breaking by a cutter assisted with rear-mounted water jet[33-34]. It should be noted that, in the actual process, the generation mechanism of lateral force is the same as the normal force, but the actual measured lateral force fluctuates around 0 due to the symmetry of the cutter. In fact,

the lateral force should not be ignored when cutter wear is studied. Therefore, it can be seen from previous experimental studies that the correct measurement of the normal load and lateral load of the cutter is the key to the study of cutter wear. **However, researching cutter wear through experiments requires huge manpower, material and financial resources, so establishing an accurate model for cutter load analysis is another key to studying cutter wear.**

At present, scholars generally use finite element [35-36]and discrete element methods [37-38] to establish a dynamic model of cutter crushing rock to analyze cutter load. For the existing finite element method simulation research on rock crushing with conical cutters [39-41], there are mainly the following shortcomings. The first is that the research on the normal and the lateral force is still ignored, and these studies only studied the cutting force. The second, because the rock elements are deleted to simulate rock failure in finite element method, the contact between the cutter and the rock is reduced when the mesh is not dense enough, and the cutter load cannot be

accurately simulated, especially the normal and the lateral force will be reduced accordingly. The third, conical cutter almost be simulated as rigid body, only the cutting force load can be obtained, and intuitive load distribution diagrams such as stress contour cannot be obtained.

The existing simulation research of the conical cutter for rock crushing using discrete element method can make up for the shortcomings of finite element method to a certain extent, but there are still shortcomings. Some scholars use 2D discrete element method for simulation [43]. The obvious disadvantage of the model established by this method is that the normal force and lateral force of the cutter cannot be simulated. But 3D discrete element method can effectively solve this problem [44], and because there are no discrete particles deleted, the rock mass still contacts the cutter, and the simulated cutter load is more realistic.But for 3D discrete element method, it is still unable to obtain an intuitive stress distribution diagram.

For the existing problems of the finite element method and the discrete element method, the SPH (Smoothed Particle Hydrodynamics) method [45-46]can be used to solve them. However, SPH methods are mostly used to simulate fluids such as water jets[47-48] and CO2 jets[49]. With the widespread use of SPH method, it is gradually used to simulate rocks[50-51]. But, there is no report about using SPH method to establish a dynamic model of cutter crushing rock mass. For the study of

rock mass broken by cutting tools, SPH method to rock can simulate the rock discrete crushing state which is difficult to simulate by FEM method. The SPH method simulating the cutting tool at the same time can better solve the tool contact with rock than the FEM-SPH coupling or the FEM-DEM coupling.Therefore, based on the SPH method, this paper establishes a three-dimensional dynamic model of cutter crushing rock mass to analyze the relationship between the cutting performance factors and cutter wear.

2. Numerical and experimental methods

To study the wear load of conical cutter, the load area on cutter should be clear firstly. The load area and components forces of cutter have been shown in reference [52] (Fig.3), and this paper will not go into details. The advancing force is usually in X--direction, while normal force in Y--direction and side force in Z--direction. For the three-dimensional model, the X-, Y-, and Z-direction cutting loads of the cutter can be obtained at the same time. However, the Z-direction cutting load is difficult to measure on one side in the actual process, and the two sides will cancel each other out during the overall measurement. Therefore, a divided cutter model is established in LS-DYNA [53-54], and the established overall three-dimensional SPH model for cutter crushing rock is shown in Fig.2(a).
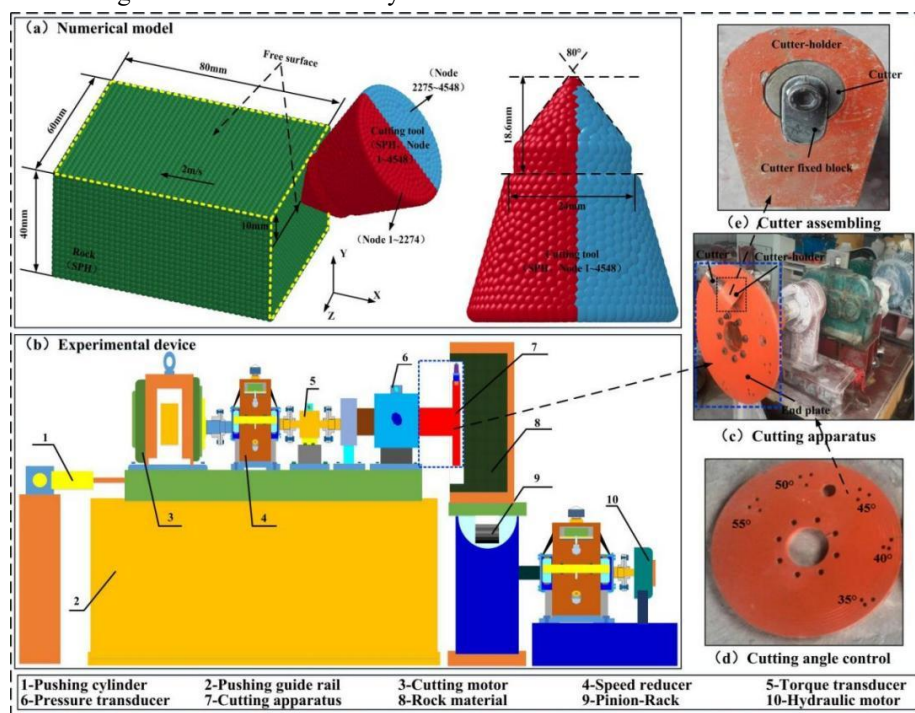

Fig.2. Numerical model and experimental device.

The numerical model adopts the m-kg-s unit system, and both the rock and the cutter are simulated by the SPH method. The rock mass is 80mm long, 60mm wide, and 40mm high. It is made of Johnson-Holmquist-Concrete material. The Mechanical parameters are given in Table 1[55]. The compress strength of the rock is 40MPa. There two free surfaces, and the other surfaces are subject to normal constraints. The height of

the cutter carbide tip is 18.6mm, the cutter tip cone angle is 80°, the cutter body end face diameter is 24mm, the inclination angle is 0°, the cutting angle is set to 35°,40°,45°,50°,55°, and the elastic material is used. All the SPH particles of the cutter is applied a constant speed V=2m/s in X-direction through the keyword BOUNDARY_PRESCRIBED_ MOTION_SET, and the cutting depth is 10mm.

Table 1. Mechanical parameters of rock.

Parameters	Values	Parameters	Values
Normalized cohesive strength A_0	0.28	Damage constant D_2	1.0
Normalized pressure hardening B_0	1.24	Amount of plastic strain before fracture E_{fmin}	0.01
Pressure hardening exponent N_0	0.84	Crushing pressure P_t（Pa）	1.6e7
Normalized Maximum strength S_{max}	15.0	Crushing volumetric strain μ_t	0.001
Strain rate coefficient C_0	0.006	Locking pressure P_1（Pa）	1.21e9
Mass density ρ_0（kg/m^3）	2410	Locking volumetric strain μ_l	0.1
Shear modulus G（Pa）	5.8e9	Pressure constant K_1（Pa）	1.2e10
Quasi-static uniaxial compressive strength $f_c^{'}$（Pa）	4.0e7	Pressure constant K_2（Pa）	1.35e10
Maximum tensile hydrostatic pressure T（Pa）	1.0e6	Pressure constant K_3（Pa）	6.89e10
Damage constant D_1	0.04		

To simulate the contact between the two SPH part, the interaction through both interpolation method and node to node contact method was adopt. The CONT=1 option in keyword *CONTROL_SPH was set, and keywords *SECTION_SPH_INTERACTION and *DEFINE_SPH_TO _SPH_COUPLING were added, shown in Table 2 and Table 3.

The wear test of the cutter is carried out on the experimental device shown in Fig. 2 (b) (c) [31]. The cutting tool is installed on the end plate and rotates with the motor. The end plate can control the cutting Angle from 35° to 55° shown in Fig. 2 (d). The rock material is fed in a straight line driven by the pinion-rack mechanism 9. The cutter cannot be rotated in the cutter-holder and is fixed by the cutter fixing block shown in Fig. 2 (e). Cutting torque can be measured by torque sensor 5 during the cutting process. The cutter wear can be observed after cutting.

Table 2. Keyword *SECTION_SPH_INTERACTION.

SECID	CSLH	HMIN	HMAX	SPHINI	DEATH	START
1	1.2	0.2	2.0	0.0	1.0e20	0.0

Table 3. Keyword *DEFINE_SPH_TO _SPH_COUPLING.

SSID	MSID	SSTYP	MSTYP	IBOX1	IBOX2	PFACT	SRAD	DFACT
1(2)	3	1	1	1	2	1.0	1.0	0.0

3. Results and discussion

3.1. Analysis of rock fragmentation and stress

The numerical simulation time is 0.03s, and the cutter advances 60mm. Fig.3 shows the three-dimensional stress distribution of rock under the action of the cutter. Fig.3 (a), (b) shows the Von-mises stress. It can be seen that in the early stage of cutting (Fig.3a), the rock mass has a compacted area, an extrusion deformation area and an extrusion stress transfer area. The compacted area is mainly distributed in front of and below the cutter, and its maximum principal stress can reach about 100MPa, which is much greater than the compressive strength of the rock. Due to the free surface effect, the extrusion deformation area mainly appears at the free surface in front of the cutter. The undeformed and unbroken rock mass after contact with the cutter is the extrusion stress transfer area, including the front, both sides and bottom of the cutter. As the cutting continues, the rock mass gradually forms large and fine-grained fragments. Among them, the large fragments are mainly formed by the extrusion in front of the cutter. The fine-grained fragments are formed by the grinding action between the cutter

and the rock. Under the action of the cutter or the collision among the large fragments, the large fragments will peel off to form small blocks and fine particles (Fig.3b).
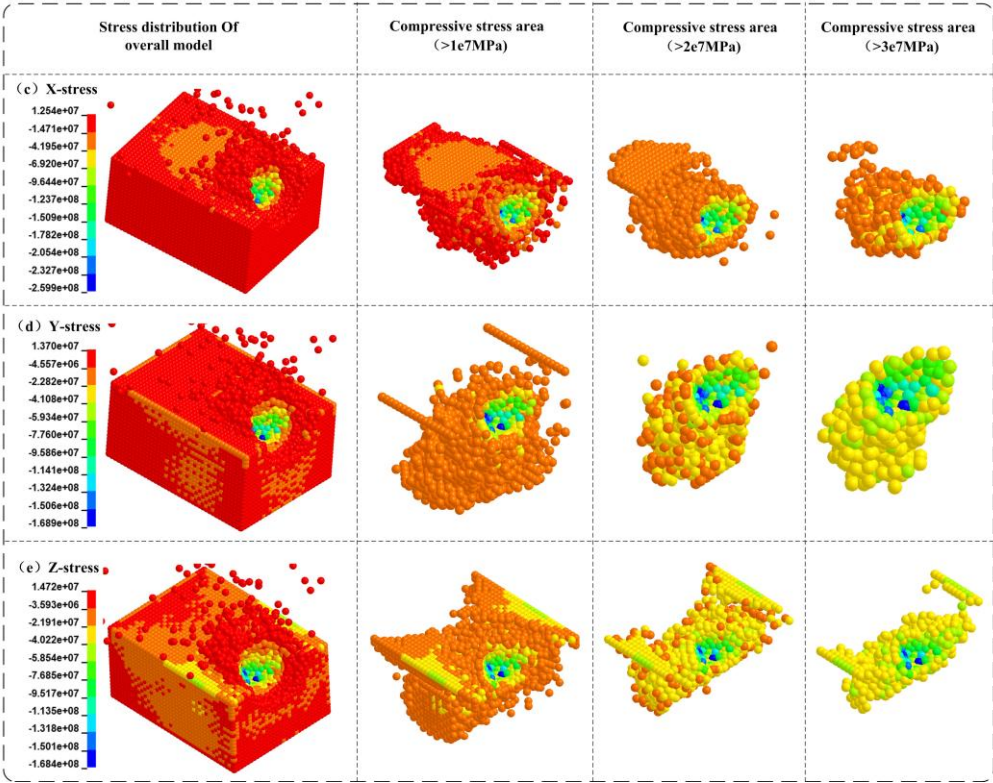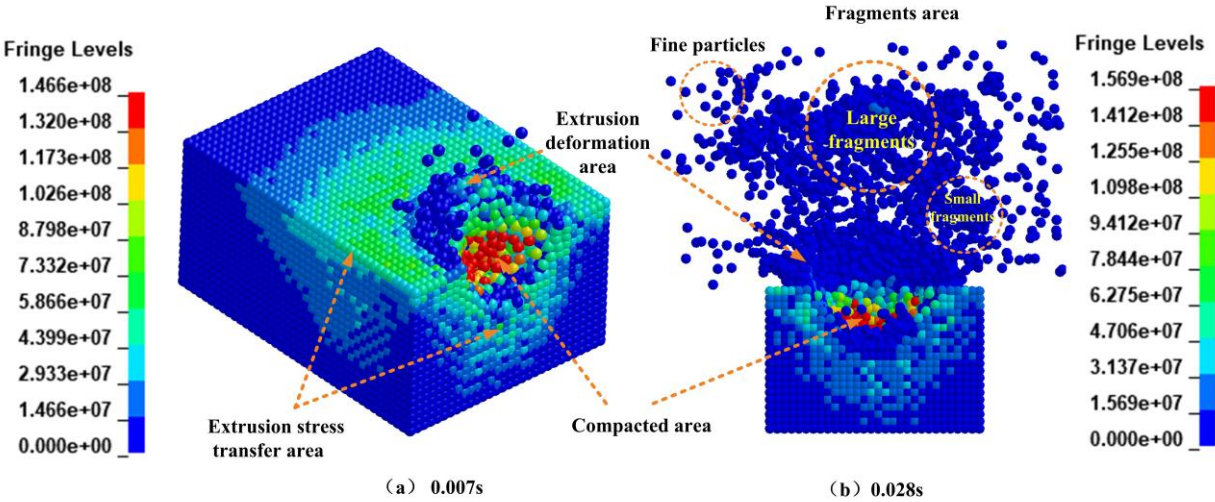

(a) 0.007s (b) 0.028s

Fig.3. Three-dimensional stress distribution of rock under the action of the cutter.

The study of rock stress distribution is indispensable for the study of cutter wear, and the distribution of compressive stress area is more important. Fig.3 also shows the three directions stress distribution of rock, where the positive value is for tensile stress, and the negative value is for compressive stress. The maximum values of the three-dimensional compressive stress are 259MPa, 168MPa and 168MPa, which far exceed the corresponding tensile strength and compressive strength of the rock. It is mainly formed by the compaction of the non-free surface. Instead of being deleted as finite elements are when they reach their limit of strength, SPH particles are always present, and they cluster together to form a denser extrusion zone with a stress value that far exceeds the compressive strength of the rock, similar to the 'dense core' theory of the tool breaking rock. And the cutter under this stress will inevitably produce huge wear with certain displacement.

In addition, Fig.3 shows the compressive stress areas with different pressure ranges in three directions. As we all know, the

conditions for friction are that two objects are in contact with each other and have relative motion. It can be seen that the X-direction compressive stress area is mainly distributed in the front of the cutter, and this direction is the same as the cutter displacement direction. It is obvious that there is no relative motion between the cutting tool and the compressive stress area in the X-direction. Thus, it has a small impact on cutter wear. The Y-direction compressive stress area is mainly distributed under the cutter, and the Z-direction compressive stress area is mainly distributed on the left and right sides of the cutter. The Y and Z directions are perpendicular to the cutter displacement direction. There are relative motions between the cutting tool and the compressive stress area in the Y and Z-direction. Therefore, this two-direction stress is the main cause of cutter

wear. The simulation results verify the analysis of conical tool wear load in reference [52] 'It should be pointed out that the reaction on area B of cutter is the main reason of wear.' The so-called area B is the compressive stress area in the Y and Z-direction.

3.2. Analysis of rock energy

In the process of forming fragments and being extruded, the rock mass has obtained certain kinetic energy and internal energy from cutter. Therefore, studying the energy of rocks helps to reveal the intrinsic relationship between tool loads and them. The kinetic energy and the internal energy of rock under different cutting angles are shown in Fig.4.

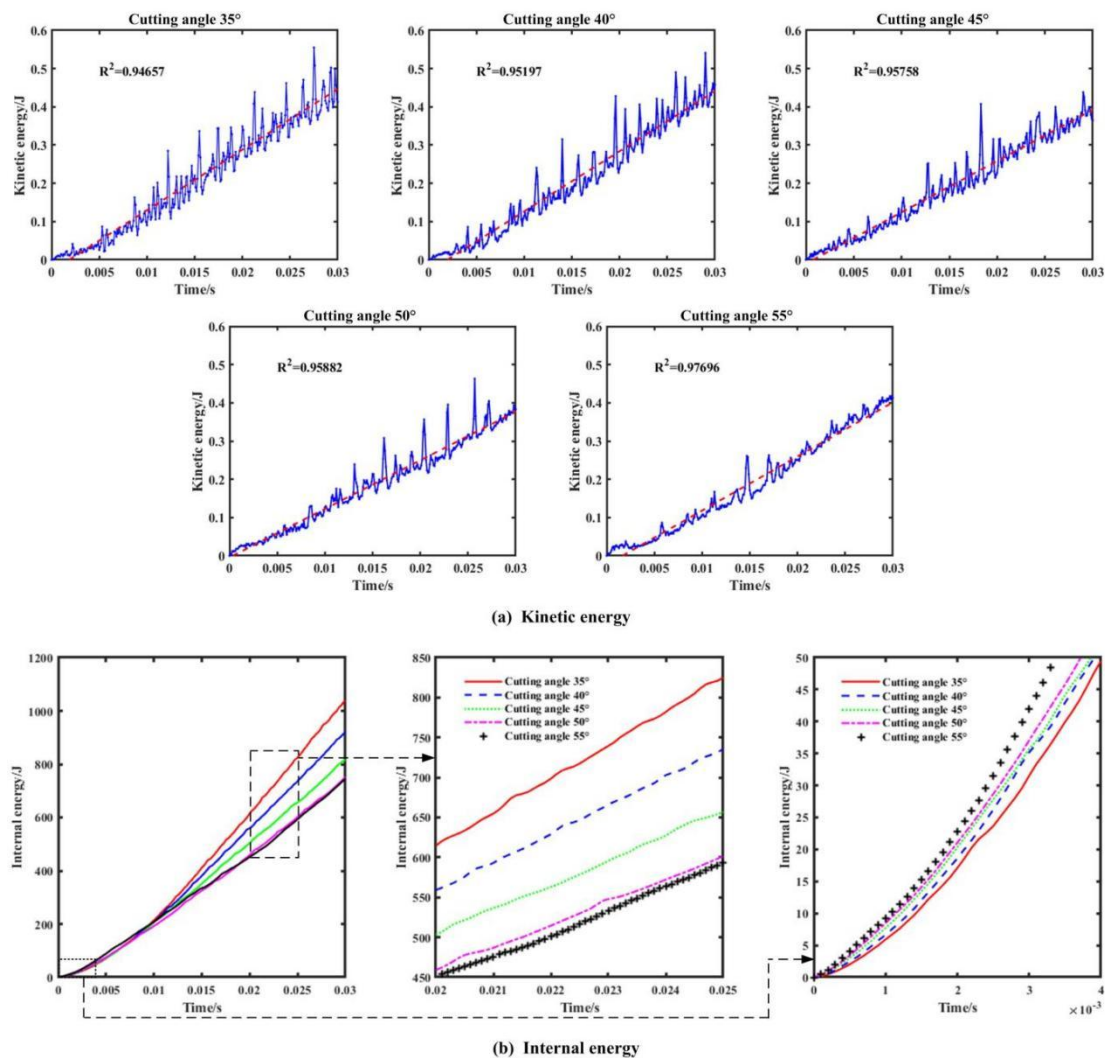(a) Kinetic energy

(b) Internal energy

Fig.4. Kinetic energy and internal energy of rock under different cutting angles.

The kinetic energy of the rock increases in a straight line with time, and the final kinetic energy obtained is about 0.4J, and the gap between different cutting angles is within 0.1J. The

kinetic energy fluctuates in different degrees during the growth process. Each fluctuation represents the splitting or avalanching of the rock mass. The greater the fluctuation, the larger the

degree of splitting or avalanching. In order to study the effect of cutting angles on rock mass splitting or avalanching, the curve is fitted and the square of the correlation coefficient is used for evaluation. It shows that with the increase of the cutting angle, the square of R gradually increases, the curve fluctuation gradually decreases, and the effect of rock mass splitting or avalanching weakens.
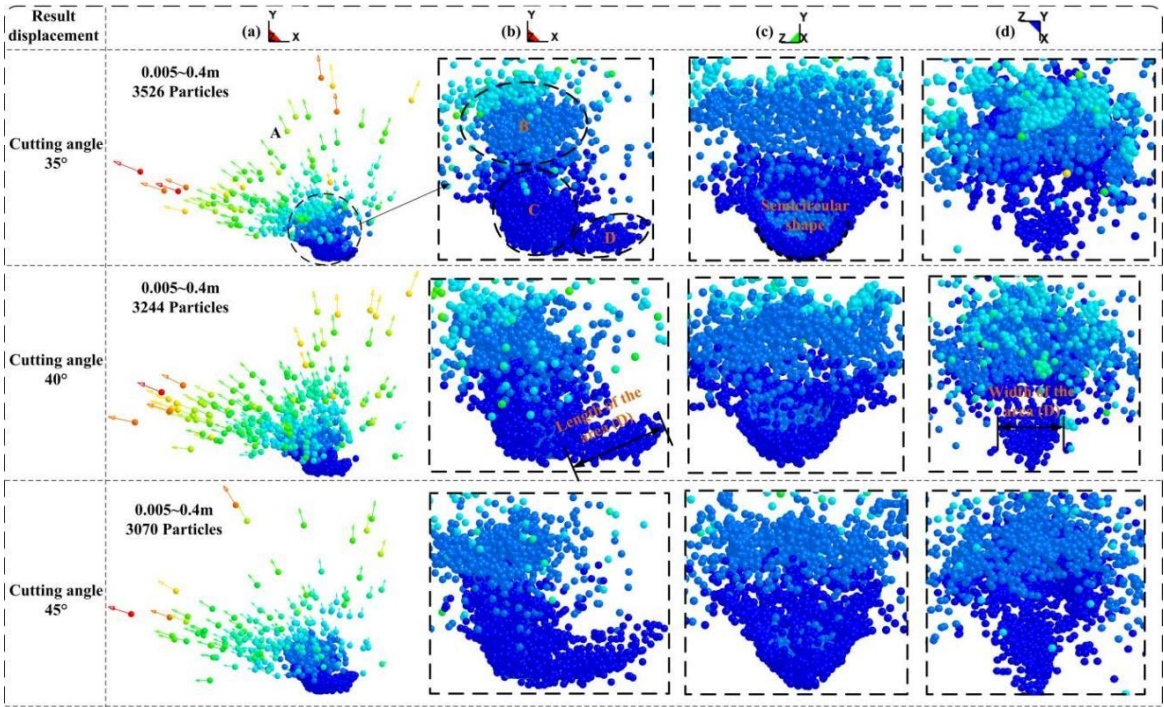
The effect of cutting angles on the rock internal energy is divided into two stages. During 0~0.01s, when the cutter tip just touches the rock mass, the smaller the cutting angle, the smaller the contact area between the cutter and the rock. In particular, the cutter with a cutting angle of 55°, where the position first contacts the rock is not the cutter tip. Therefore, the internal energy obtained by the rock mass increases with the cutting angle. As the cutter advances further, the smaller the cutting angle, the larger the contact area between the cutter and the rock. In particular, the cutter with a cutting angle of 35°, where the back face of the cutter contacts the rock mass in a large area. Therefore, the internal energy obtained by the rock mass increases with the cutting angle during 0.01~0.03s.

The effect of cutting angles on the rock internal energy is divided into two stages. During 0~0.01s, when the cutter tip just

touches the rock mass, the smaller the cutting angle, the smaller the contact area between the cutter and the rock. In particular, the cutter with a cutting angle of 55°, where the position first contacts the rock is not the cutter tip. Therefore, the internal energy obtained by the rock mass increases with the cutting angle. As the cutter advances further, the smaller the cutting angle, the larger the contact area between the cutter and the rock. In particular, the cutter with a cutting angle of 35°, where the back face of the cutter contacts the rock mass in a large area. Therefore, the internal energy obtained by the rock mass increases with the cutting angle during 0.01~0.03s.

3.3. Displacement characteristics of rock particles

In the process of cutting the rock, the cutter made the rock avalanching and deforming. At the same time, the cutter is also subjected to the reaction of the rock, and in fact the magnitude of the reaction force is more dependent on the number of the rock particles with significant displacement (>0.005m). Therefore, the displacement distribution cloud diagram and number statistics of particles displacement greater than 0.005m under different cutting angles at 0.012s are given in Fig.5.
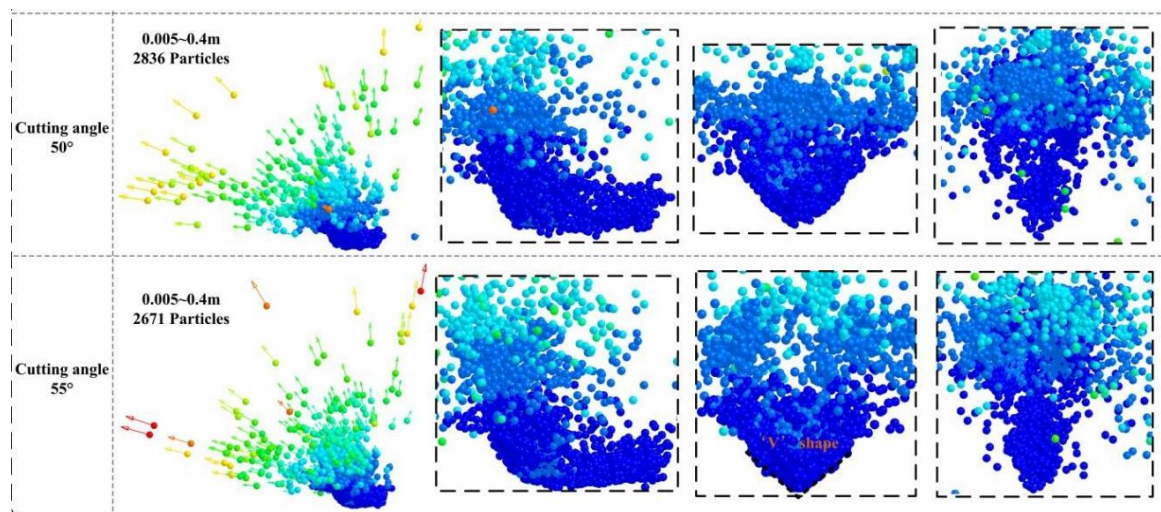
Fig.5. Displacement distribution cloud diagram and number statistics of particles displacement greater than 0.005m under different cutting angles at 0.012s.

With the cutting angle increases, the number of particles with a displacement greater than 0.005m gradually decreases, which is the same as the change trend of internal energy under different cutting angles. The rock particles with significant displacement can be further subdivided into four areas, which are mainly composed of splash area (A), fragmentation avalanching area (B), extrusion area (C) and cutter tip grinding area (D). The splash area (A) is where small particles avalanching or splashing, and they are mainly displaced in the negative X direction and the positive Y direction, shown in column (a). The fragmentation avalanching area (B) is the avalanche of larger fragments shown in the column (b). The

fragmentation of the particles in this area is affected by the cutting angle. For a small cutting angle (35°), the overall fragmentation is formed, as the cutting angle increases to 55°, the original overall avalanche gradually forms small avalanches on both sides, shown in column (c). The extrusion area (C) is distributed in front of the cutter, and it mainly moves in the negative X direction. It is related to the projection area of the cutter on the YOZ plane. The greater the projection area, the larger the extrusion area. The extrusion area is the largest for a small cutting angle (35°), shown in column (c).

Fig. 6 shows the comparison of the cutter projection on YOZ plane and broken pit shape between cutting angle 35° and 55°.
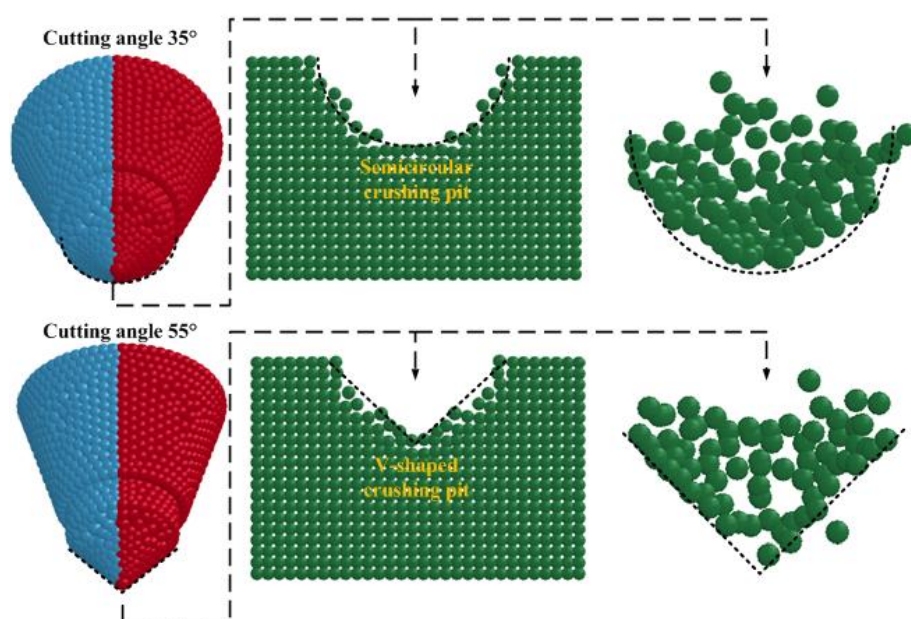

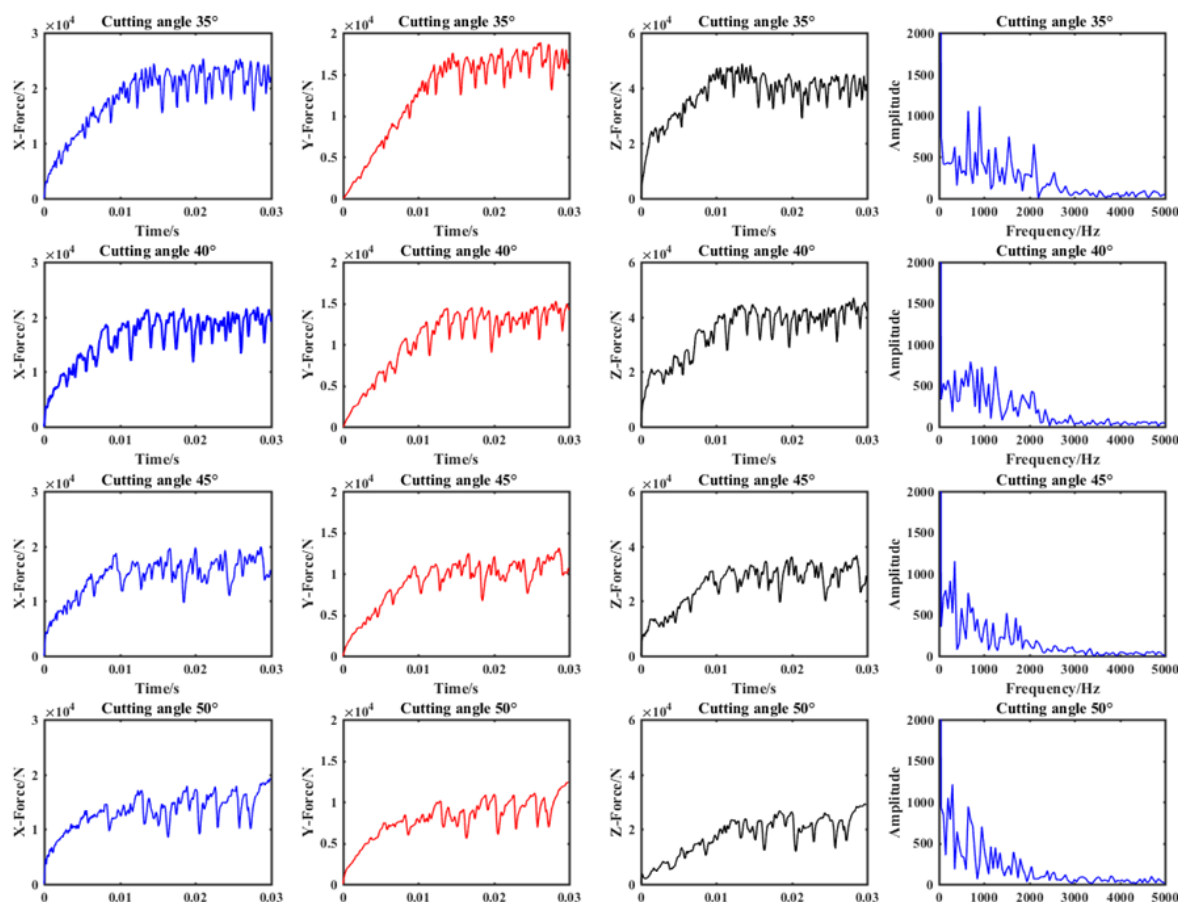Fig.6. Comparison of the cutter projection on YOZ plane and broken pit shape between cutting angle35° and 55°.

When the cutting angle is 35°, the projection profile of the cutter tip is a semicircle, and correspondingly it forms a semicircle shaped broken pit and avalanche. When the cutting angle is 55°, the projected contour at the cutter tip is V-shaped, and correspondingly, it forms a V-shaped pit and avalanche. The cutter tip grinding area (D) mainly refers to the area of splashed rock particles formed after the cutter tip interacts with the rock below the cutter tip. The length of the splashed area gradually increases with the cutting angle, shown in column(b). The main reason is that, the space between the back face of the cutter and the rock increases with the cutting angle, and the rock particles after grinding are more likely to splash. It can be seen that the more particles splashing, the less the contact between the rock and the back face of the cutter. However, the width of the splashed area does not change much after grinding shown in column (d).

3.4. Cutting load

The cutting force in X, Y and Z directions of the cutter obtained by superimposing reaction forces is shown in Fig.7. As the cutter advances gradually, the three-direction cutting force gradually rises from zero, and then stabilizes. The X-direction force is analyzed by frequency spectrum, shown in Fig.7(d).

The X-direction force includes not only the cutting force formed by the extrusion of the cutter and the rock in front of the cutter, but also the frictional force formed by the friction between the cutter and the lateral rock. However, since the X-direction force is in the same as the direction of the cutter movement, it is not the main force result in cutter wear. The Y-direction force is the result of the superposition of the positive Y-direction load on the cutter back face and the negative Y-direction load on the rake face. The load on the cutter rake face produces a normal force in the negative Y direction. However, the Y-direction force is actual in the positive Y direction. It can be seen that the load on the back face of the cutter is greater than the load on the rake face. Moreover, this load is perpendicular to the direction of the cutter movement and is one of the main loads that cause cutter wear. In the same way, the Z-direction force is the load formed by the extrusion of the cutter on the lateral rock. The combined Z-direction force on both sides of the cutter is small, but the unilateral Z-direction force is extremely large, and the load is also perpendicular to the direction of the cutter movement and is also one of the main loads causing cutter wear.
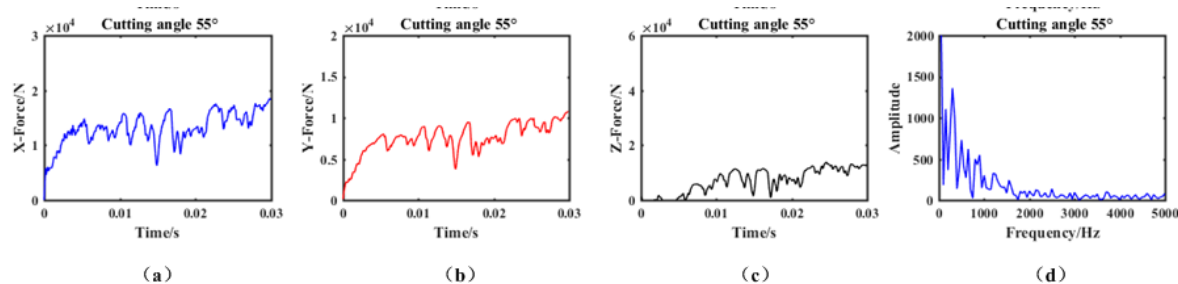
Fig.7. Three-direction cutting force of cutter crushing rock.

The values after 0.01s are selected for statistics, and the mean value and variance of the three-direction load under different cutting angles are obtained.The effect of the cutting angle on the three-direction cutting force of the cutter is shown in Fig.8(a).

When the cutting angle is 55°, the X-direction force is the largest, about 14kN, followed by the Z-direction force, and the Y-direction force is the smallest. For other cutting angles, the Z-direction force is the largest, the maximum Z-direction force is 41kN, followed by the X-direction force, and the Y-direction force is still the smallest. Compared with the reference [32], it is shown that the use of finite element method to simulate tool

cutting rock will indeed lead to a small calculated load. In the reference [32], the z-direction load is smaller than that of Y-direction, indicating that if the elements are deleted after failure, the contact between the tool and the rock is indeed reduced, thus reducing the tool load.. The three-direction force decreases with the cutting angle. Among them, the Z-direction force decreases the most. The main reason is that the contact between the cutter and the rock decreases with the cutting angle. This trend is consistent with the previous analysis that the trend of the rock mass energy and the particle displacement distribution under different cutting angles.
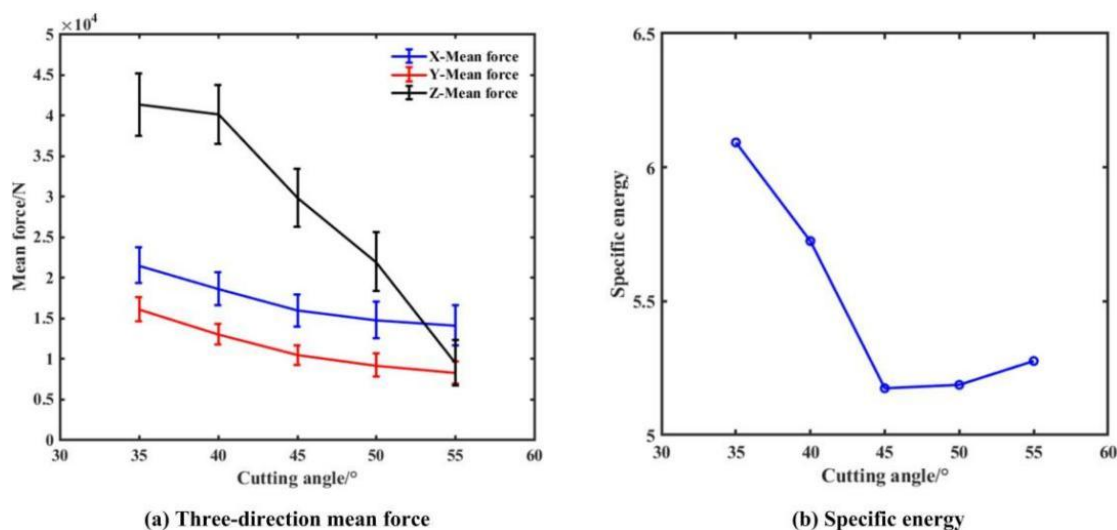

Fig.8. Effect of the cutting angle on the three-direction mean force and the specific energy.

From the above analysis, it can be seen that, for example, the cutting force of a 35° cutting angle is the largest, and the broken rock mass is also large. Therefore, the cutting performance of different cutting angles can be measured in the form of specific energy consumption. The specific energy consumption can be calculated by the ratio of the cutting resistance (X-direction force) and the corresponding number of particles with significant displacement (Fig.5). Fig.8(b) shows the effect of the cutting angle on the energy consumption. The

specific energy consumption is the smallest at 45°, significantly reduces before 45°, and slightly increases after 45°.

In addition，with the cutter advancing gradually, there is still a certain fluctuation in the cutting force curve, which is mainly caused by the rock avalanching under the action of the cutter. The rock avalanching causes the contact between the cutter rake face and the rock to decrease, which leads to a decrease for the cutting force. Through the statistics of the variance of the cutting force of the cutter, it shows that for the

three-directional force, the fluctuation amplitude under the cutting angle of 45° is relatively small; through the analysis of the frequency spectrum, the fluctuation magnitude of the cutter load decreases with the cutting angle at frequency 2000 Hz. The main reason is still the reduction of the contact between the cutter and the rock.
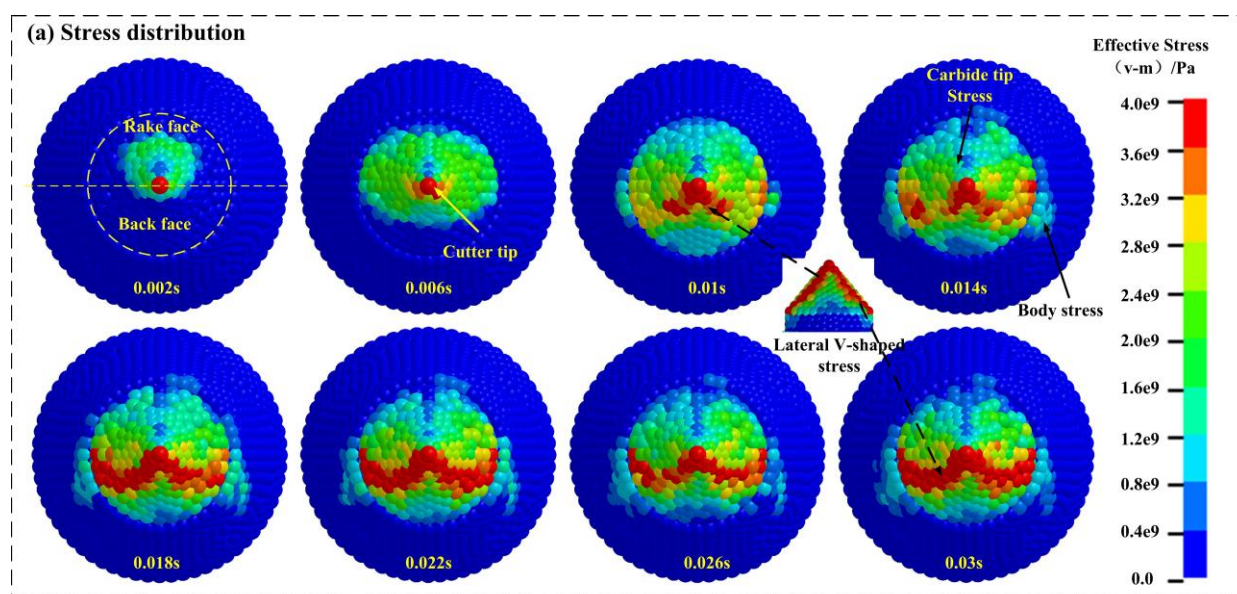
3.5. Cutter stress distribution

The cutter stress cloud diagram distribution in the time domain can be obtained during the cutting process, shown in Fig.9.

In the initial stage of cutting (<0.002s), only the cutter rake face is in contact with the rock, so that the increase in cutter stress is mainly concentrated on the rake face, while the back face has almost no stress distribution. As the cutter advances gradually, on one hand, there is both the increase in cutter stress on the rake face and the back face. The increase in cutter stress on the rake face is produced by the extrusion between the cutter and rock in the front of the cutter, while that on the back face is produced by the extrusion and friction between the cutter and the rock below the cutter. When the cutter completely cuts into the rock, the stress area of the back face gradually increases, and sometimes it is the main stress distribution area of the entire cutter. This is mainly because the back face of the cutter is in continuous contact with the rock, but the rock mass in front of the cutter is easy to avalanche to cause the decreasing of the contact between rake face and the rock, which results in a relative decrease in the stress of the rake face. On the other hand, due to interference, some stresses appear in the cutter body. As the cutter gradually enters the cutting, the interference between the cutter body and the rock increases, and the stress area gradually increases.

In order to further analyze the time-domain characteristics of cutter stress distribution, it should be focus on the four stress areas of the cutter tip, rake face, back face and cutter side (the interference area between the cutter and the V-groove of the rock). It can be seen that the stress at the cutter tip are the largest in the entire time domain, followed by that at the cutter side, again that at the back surface, and finally that at the rake face. For the cutter side, it forms a V-shaped stress areas, which is mainly caused by the Z-direction force.

Furthermore, the effect of cutting angles on cutter stress distribution is shown in Fig.10. With the increase of the cutting angle, the V-shaped stress area on the cutter side gradually narrows, mainly caused by the reduction of the interference between the two sides of the cutter and the V-groove of rock. This is consistent with the analysis in reference [16]. The stress area of the back face gradually decrease, which is mainly caused by the reduction of the extrusion between the bottom of the cutter and the rock. At 50° and 55°, the contact between the upper part of the cutter rake face and the rock increases, so that the upper part of the stress area of the rake face gradually increases. The stress area of the cutter body gradually becomes shorter, which is mainly caused by the reduction of the interference between the body and the rock.
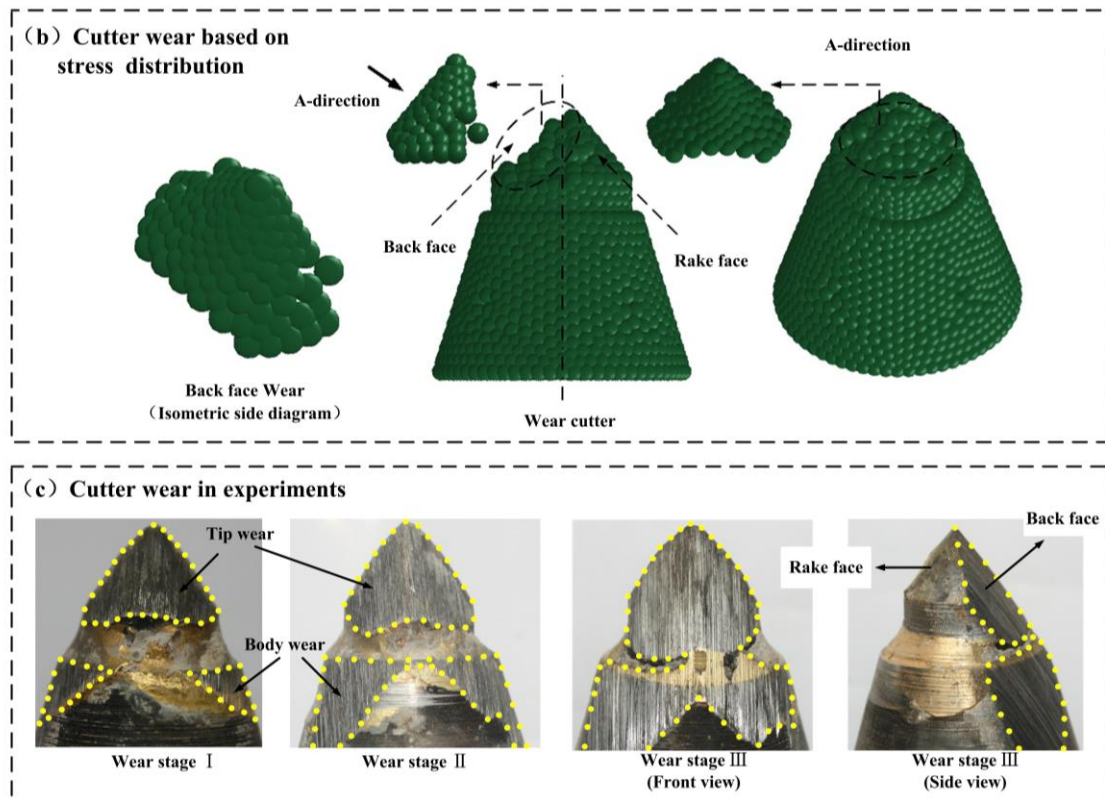

(a) Stress distribution

Fig.9. Evolution of cutter stress cloud diagram in time domain.
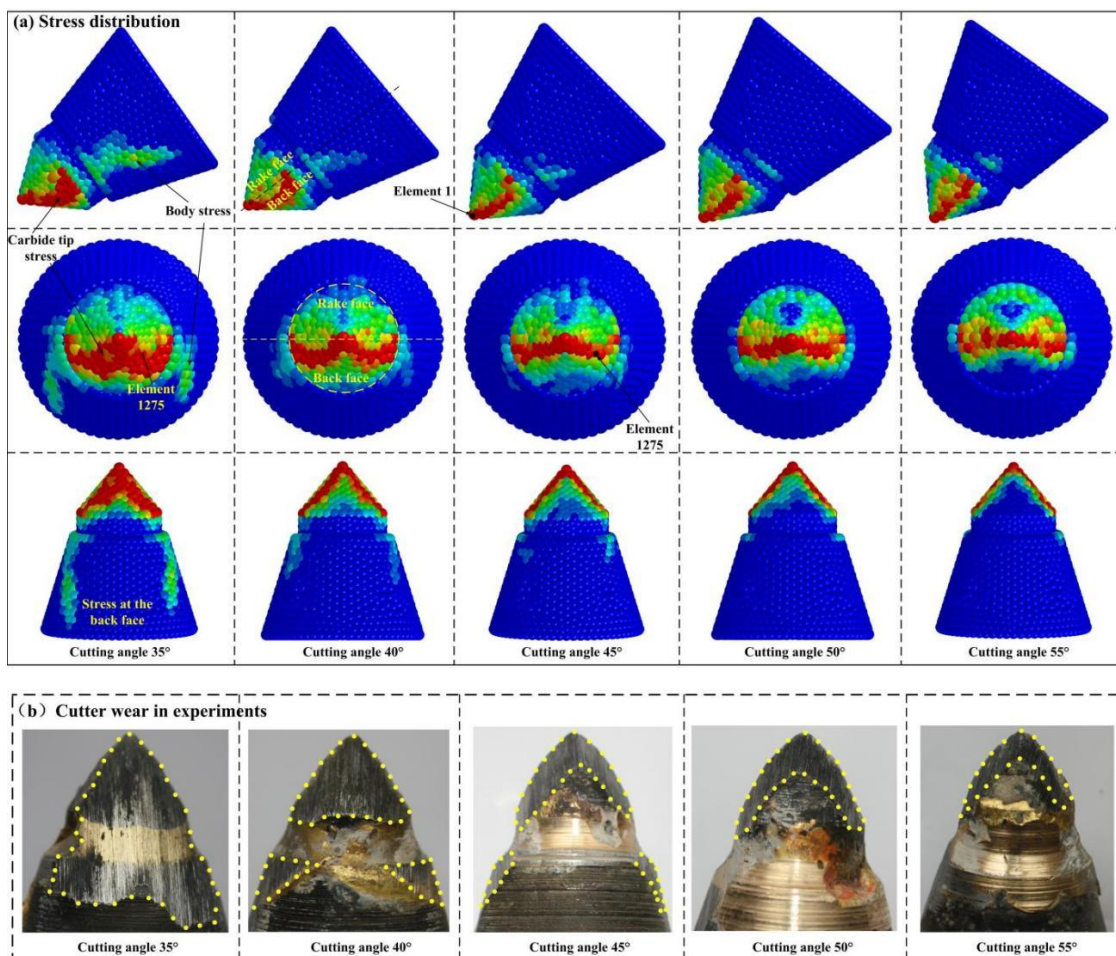

Fig.10. Effect of cutting angles on cutter stress distribution.

Since the cutter tip and the cutter side are where the stress are greatest, they will wear and fail at the earliest, and their failure will affect the failure of the other positions of cutter. Therefore, the stress of the two places should be focused on specially. Fig.11 shows the effect of cutting angles on the stress at the tip and side of the cutter in time domain. The cutter tip stress are given by Element 1, the cutter side stress are given by Element 1275. The data of the cutter tip stress after 0.005s are taken to calculate the mean value, while the data after 0.01s are taken for cutter side.

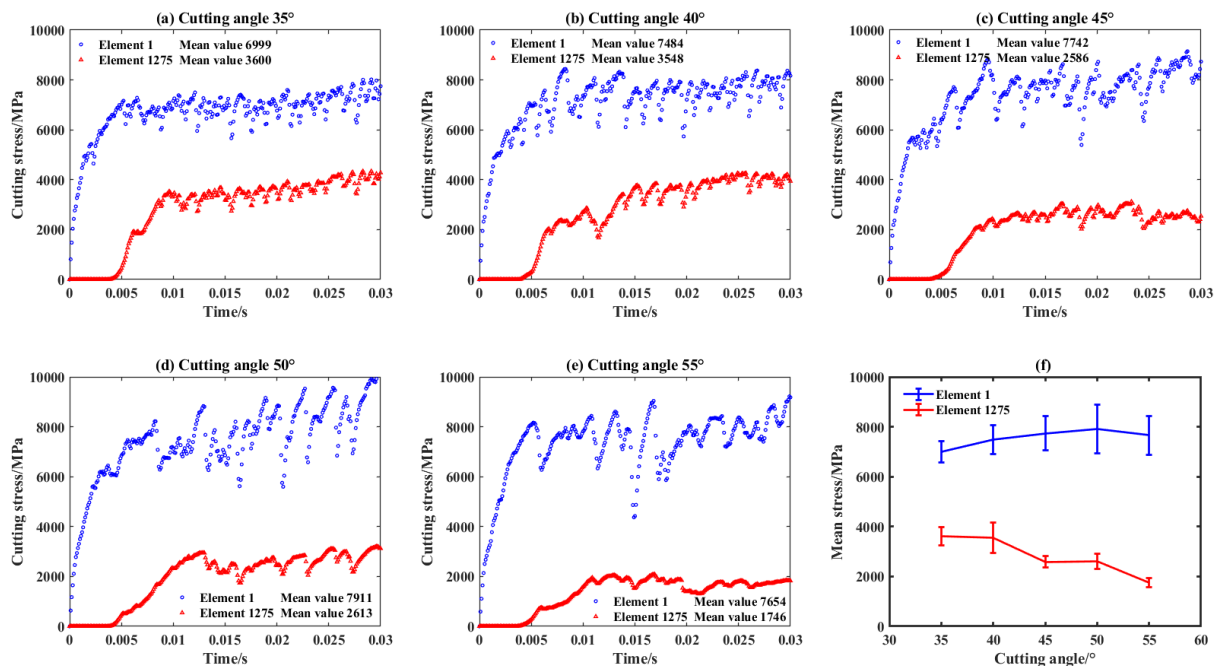Similar to the fluctuation frequency of the cutting force, the stress fluctuation frequency of the cutter tip and cutter side gradually decrease with the cutting angle. For the cutter tip stress, the average value gradually increases with the cutting angle (35°~50°), and the fluctuation amplitude also gradually increases. Since the tip of the cutter is not the first part to contact the rock mass at 55°, the tip stress are relatively small. For the cutter side stress, with the increase of the cutting angle, the average value gradually decreases, among which the change from 40° to 45° and the change from 50° to 55° are large. In addition, the fluctuation is the smallest at 45° (Except for 55°).

Fig.11. Effect of cutting angles on the stress at the tip and side of the cutter in time-domain.

4. Conclusions

By comparing the simulation results of stress distribution with the actual tool wear, it can be seen that the dynamic model of cutter crushing rock established by SPH method can effectively simulate the loading of the cutter during the cutting process, and it can be correct to predict cutter wear according to the loading. In particular, it can accurately extract the direct load-side load that causes cutter wear, which is difficult to measure directly in the test. The specific conclusions are as follows:

(1) The kinetic energy of the rock mass increases in a straight line with time and fluctuates greatly; the degree of fluctuation reflects the avalanching effect of the rock mass. The research results show that the smaller the cutter cutting angle, the better the avalanching effect of the rock mass. The effect of the cutter on the internal energy of the rock mass is divided into two stages. One is when it just touches the rock, and the other is when it gradually enters the cutting. The influence trends of the two are different, but both reflect that the internal energy of the rock mass is positively correlated to the contact area between the cutter and the rock, and the larger the area, the greater the internal energy. Furthermore, the internal energy of the rock can be characterized by rock particles with significant displacement (>5mm). As the cutting angle increases, the number of particles with a displacement greater than 5mm gradually decreases, which is consistent with the change trend of internal energy.

(2) Except for 55°, all the Z-direction forces are largest under other cutting angle conditions, the largest Z-direction force is 41kN, followed by the X-direction force, and the Y-direction force is the smallest. The three-direction force

decreases with the cutting angle, which is consistent with the change trend of internal energy and rock particles with significant displacement, indicating that internal energy, rock deformation and cutter load can be characterized by each other. In order to study the cutting performance of the tool, the specific energy consumption is defined by the ratio of the cutting resistance (X-direction force) and the corresponding number of particles with significant displacement. It indicates that under the condition of the given cutter structure, the specific energy consumption is the lowest at a cutting angle of 45°, and there is little difference at 50°.

(3) There is a certain fluctuation for the cutting force in the cutting process. The fluctuation magnitude of the cutter load decreases with the cutting angle at frequency 2000 Hz. The fluctuation amplitude is represented by the variance statistics of the cutting force. When the cutting angle is 45°, the fluctuation amplitude of the three-directional force is the smallest, followed by 40°.

(4) From evolution of cutter stress cloud diagram in time domain, The stress at the cutter tip are the largest in the entire time domain, followed by that at the cutter side. Therefore, the stress of the two places should be focused on specially. For the cutter tip stress, the average value gradually increases with the cutting angle (35°~50°), and the fluctuation amplitude also gradually increases. For the cutter side stress, the average value gradually decreases with the cutting angle, among which the change from 40° to 45° and the change from 50° to 55° are large. In addition, the fluctuation is the smallest at 45° (Except for 55°).

Based on the above conclusions, under the conditions of the cutter structure in this paper, the selection reference of cutting angles for different consideration factors is shown in Table 4.

Table 4. Selection reference of cutting angles for different consideration factors.

Cutting angles	Specific energy consumption	Load fluctuation	Avalanching performance or stress at cutter tip	Cutting load or stress at cutter side
35°	—	—	Optimal	—
40°	—	Second	Second	—
45°	Optimal	Optimal	Optional	Optional
50°	Second	Optional	—	Second
55°	Optimal	—	—	Optimal

Among them, there is a causal relationship between factor avalanching performance and factor stress at cutter tip. `When selecting the cutting angle, the results are consistent. Therefore, it can be regard as one factor, and the optimal angle is 35°, followed by 40°, and finally 45° is optional. Similarly, the cutting load or stress at cutter side are considered as one factor. The optimal angle is 55°, followed by 50°, and finally 45° is optional. For factor specific energy consumption, the optimal angle is 45°, followed by 50°, and finally 55°. If the factor load fluctuation is considered, the optimal angle is 45°, followed by 40°, and finally 45° is optional. Considering all 4 factors, the

optimal angle is 45°, followed by 50°. There are two factors directly related to wear, one is the stress at cutter tip, and the other is the stress at cutter side. The two are affected by the cutting angle in the opposite way. Although the cutter side area is larger than the cutter tip area when the cutter is first used, as the cutter wears, the cutter tip area will continue to increase, and the cutter tip and the cutter side are equally important to the wear of the cutter. Therefore, it is recommended to choose 45°. Although the wear performance of the two areas is not optimal, it will not produce excessive wear.

References

1. Su, O., and Akkas. M.Assessment of pick wear based on the field performance of two transverse type roadheaders: a case study from Amasra coalfield. B. Eng. Geol. Environ 2020; 79(5): 2499-2512. https://doi.org/10.1007/s10064-019-01712-x

2. Lu, Z.G., Wan L R, Zeng Q L, Zhang X, and Gao K D. The structural optimization of roadheader conical picks based on fatigue life. Int. J. Simul. Model 2018;9 (2): 1850013. https://doi.org/10.1142/s1793962318500137

3. Evans, I. A theory of the picks cutting force for point-attack. Int. J. Min. Eng 1984; 2(1): 63–71. https://doi.org/10.1007/BF00880858

4. Roxborough, F.F., and Liu Z C. Theoretical considerations on pick shape in rock and coal cutting. In Proceedings of the sixth underground operator's conference. Kalgoorlie 189(1995):193.

5. Goktan, R.M. A suggested improvement on Evans' cutting theory for conical bits. In Proceedings of fourth symposium on mine mechanization automation. Brisbane 1 (1997): 57–61.

6. Goktan, R.M., and Gunes N. A semi-empirical approach to cutting force prediction for point-attack picks. J. South Afr. Inst. Min. Metall., 105(02): 257–263.

7. Bilgin, N, ADemircin M, Copu H, Balci C, Tuncdemir H, and Akcin N A. Dominant rock properties affecting the performance of conical picks and the comparison of some experimental and theoretical results. Int. J. Rock. Mech. Min. Sci 2006; 43(1): 139–156. https://doi.org/10.1016/j.ijrmms.2005.04.009

8. Yasar, S., and Yilmaz A O. Drag pick cutting tests: A comparison between experimental and theoretical results. J. Rock Mech. Geotech 2018; 10(05): 893-906. https://doi.org/10.1016/j.jrmge.2018.02.007

9. Li, X., Wang S, Ge S, Malekian R, and Li Z. A Theoretical Model for Estimating the Peak Cutting Force of Conical Picks. Exp. Mech 2018; 58(5): 709-720. https://doi.org/10.1007/s11340-017-0372-1

10. Yasar, S. A general Semi-Theoretical model for conical picks. Rock Mech. Rock. Eng 2020; 53: 2557-2579. https://doi.org/10.1007/s00603-020-02078-3

11. Wang, X., and Su O. Specific energy analysis of rock cutting based on fracture mechanics: A case study using a conical pick on sandstone. Eng. Fract. Mech 2019; 213: 197-205. https://doi.org/10.1016/j.engfracmech.2019.04.010

12. Wang, X., Wang Q F, Liang Y P, Su O, and Yang L. Dominant cutting parameters affecting the specific energy of selected sandstones when using conical picks and the development of empirical prediction models. Rock. Mech. Rock. Eng 2018; 51(10): 3111-3128. https://doi.org/10.1007/s00603-018-1522-1

13. Yu, B. Numerical Simulation of Continuous Miner Rock Cutting Process. West Virginia University;2005.

14. Mishra, B. Analysis of Cutting Parameters and Heat Generation on Bits of a Continuous Miner Using Numerical and Experimental Approach. West Virginia University;2007.

15. Liu, S.Y., Du C L, and Cui X X. Research on the cutting force of a pick. Min. Sci. Technol 2009;19 (4): 514–517 (China). https://doi.org/10.3969/j.issn.2095-2686.2009.04.020,

16. Liu, X.H., Liu S Y, Cui X X, and Tang P. Interference model of conical pick in cutting process. J. Vibroeng 2014; 16 (1): 115–128.

17. Liu, S.Y., Cui Y M , Chen Y Q, and Guo C W. Numerical research on rock breaking by abrasive water jet-pick under confining pressure. Int. J. Rock. Mech. Min. Sci 2019; 120: 41-49. https://doi.org/10.1016/j.ijrmms.2019.06.007

18. Li, H.S., Liu S Y, and Xu P P. Numerical simulation on interaction stress analysis of rock with conical picks. Tunn. Undergr. Space. Technol 2019; 85: 231-242. https://doi.org/10.1016/j.tust.2018.12.014

19. Liu, S.Y., Zhou F Y, Li S H, Chen Y Q, Wang F C, and Guo C W. Experimental Investigation of Hard Rock Breaking Using a Conical Pick Assisted by Abrasive Water Jet. Rock. Mech. Rock. Eng 2020; 53:, 4221–4230. https://doi.org/10.1007/s00603-020-02168-2

20. Yasar, S. Determination of optimum rock cutting data through single pick cutting tests. Geotech. Lett 2019; 9(1): 8-14. https://doi.org/10.1680/jgele.18.00124

21. Qiao, S., Xia J Y, Xia Y M, Liu Z Z, Liu J S, and Wang A L. Establishment of coal-rock constitutive models for numerical simulation of coal-rock cutting by conical picks. Period. Polytech.-Civ 2019; 63(2): 456-464. https://doi.org/10.3311/PPCI.13084

22. Huang, J., Zhang Y M, Zhu L S, and Wang T. Numerical simulation of rock cutting in deep mining conditions. Int. J. Rock Mech. Min. Sci 2016; 84: 80–86. https://doi.org/10.1016/j.ijrmms.2016.02.003

23. Dewangan, S., and Chattopadhyaya S. Performance analysis of two different conical picks used in linear cutting operation of coal. Arab. J. Sci. Eng 2016; 41: 249–265. https://doi.org/10.1007/s13369-015-1786-7

24. Wang, S.F., Li X B, Yao J R, Gong F Q, Li X, Du K, Tao M, Huang L Q, and Du S L. Experimental investigation of rock breakage by a conical pick and its application to non-explosive mechanized mining in deep hard rock. Int. J. Rock Mech. Min. Sci 2019; 122: 10406. https://doi.org/10.1016/j.ijrmms.2019.104063

25. Wang, S.F.,.Li X B, Du K, and Wang S Y. Experimental investigation of hard rock fragmentation using a conical pick on true triaxial test apparatus. Tunn. Undergr. Space Technol 2018; 79: 210-223. https://doi.org/10.1016/j.tust.2018.05.006

26. Zhang, Q.Q., Han Z N, Zhang M Q, and Zhang J G. Experimental and numerical simulation study on the wear of tapered pick under impact load. J. Vib. Shock 2016; 35(13): 58-65.

27. Fan, Q.X., Zhang Q Q, Liu G R, Li X, Jia W, Guo Z W, and Han R M. An experimental study on wearing of conical picks interacting with rock. T. Can. Soc. Mech. Eng 2019; 43(7): 544-550. https://doi.org/10.1139/tcsme-2018-0225

28. Fan, Q.X., Zhang Q Q, and Liu G R. A stress analysis of a conical pick by establishing a 3D ES-FEM Model and using experimental measured forces. Appl. SCI 2019; 9(24): 5410. https://doi.org/10.3390/app9245410

29. Yang, D.L., Li J P, Wang L P, Gao K D, Tang Y L, and Wang Y X. Experimental and theoretical design for decreasing wear in conical picks in rotation-drilling cutting process. Int. J. Adv. Manuf. Technol 2015; 77: 1571-1579. https://doi.org/10.1007/s00170-014-6472-5

30. Yang, D.L., Li J P, Zheng K H, Jiang H X, Xu H D, and Liu S Y. High-hardness alloy substituted by low hardness during drilling and cutting experiments of conical pick. Int. J. Rock Mech. Min. Sci 2017; 95: 73-78. https://doi.org/10.1016/j.ijrmms.2017.04.006

31. Liu, S.Y., Ji H F, Liu X H, and Jiang H X. Experimental research on wear of conical pick interacting with coal-rock. Eng. Fail. Anal 2017; 74: 172-187. https://doi.org/10.1016/j.engfailanal.2017.01.013

32. Liu, X.H., Tang P, Geng Q, Li X, and Tian M R. Numerical research on wear mechanisms of conical cutters based on rock stress state. Eng. Fail. Anal 2019; 97: 274-287. https://doi.org/10.1016/j.engfailanal.2019.01.045

33. Liu, S.Y., Liu X H, Chen J F, and Lin M X. Rock breaking performance of a pick assisted by high-pressure water jet under different configuration modes. Chin. J. Mech. Eng 2015; 28 (3): 607–617. https://doi.org/10.3901/CJME.2015.0305.023

34. Liu, S.Y., Ji H F, Han D D, and Guo C W. Experimental investigation and application on the cutting performance of cutting head for rock cutting assisted with multi-water jets. Int. J. Adv. Manuf. Technol 2018; 94: 2715-2718. https://doi.org/10.1007/s00170-017-1072-9

35. Feng, C.C., Liu W, and Gao D L. CFD simulation and optimization of slurry erosion of PDC bits. Powder. Technol 2022; 408: 117658. https://doi.org/10.1016/J.POWTEC.2022.117658

36. Zheng, K.H., Qiu B J, Wang Z Y, Li J P, and Gao K D. Modelling heterogeneous coal-rock (HCR) failure patterns under dynamic impact loads using image-based finite element (FE) and discrete element (DE) model. Powder. Technol 2020; 360: 673-682. https://doi.org/10.1016/j.powtec.2019.10.036

37. Liu, S., Huang H, Qiu T, and Gao L. Comparison of laboratory testing using smartrock and discrete element modeling of ballast particle movement. J. Mater. Civil. Eng 2016; 29(3): D6016001. https://doi.org/10.1061/(ASCE)MT.1943-5533.0001540

38. Gong, F.Y., Deng R, Wang Q H, Bai J W, and Cheng X J. Influence of aggregate motion related to rutting depth of

asphalt mixture based on intelligent aggregate and DEM. J. Mater. Civil. Eng 2024; 36(5): 04024056. https://doi.org/10.1061/JMCEE7.MTENG-17165

39. Liu, S.Y., Ji H F, and Liu X H. Effect of pick working angle on the cutting performance of a cutting head. J. Braz. Soc. Mech. Sci 2017; 39(10): 4147-4159. https://doi.org/10.1007/s40430-017-0806-9

40. Jiang, H.X., and Meng D G. 3D numerical modelling of rock fracture with a hybrid finite and cohesive element method. Eng. Fract. Mech 2018; 199: 280-293. https://doi.org/10.1016/j.engfracmech.2018.05.037

41. Jiang, H.X., Du C L, and Dong J H. Investigation of rock cutting dust formation and suppression using water jets during mining. Powder. Technol 2017; 307: 99-108. https://doi.org/10.1016/j.powtec.2016.11.029

42. Liu, X.H., Liu S Y, and Ji H F. Mechanism of rock breaking by pick assisted with water jet of different modes. J. Mech. Sci. Technol 2015; 29(12): 5359-5368. https://doi.org/10.1007/s12206-015-1137-3

43. He, B., Shao W, Tang J Y, Zong X M, and Kang K X. The Effect of Pick Profile on the Cutting Performance of Point Attack Picks. Key. Eng. Mater 2018; 789: 31-36. https://doi.org/10.4028/www.scientific.net/KEM.789.31

44. Wyk, G.V., Els D N J, Akdogan G, Bradshaw S M, and Sacks N. Discrete element simulation of tribological interactions in rock cutting. Int. J. Rock Mech. Min. Sci 2014; 65: 8-19. https://doi.org/10.1016/j.ijrmms.2013.10.003

45. Lai, Zh J, Li H J, Yin X X, Zhou J H, Zheng X B, and Yang H R. Properties and Simulation of UHPC and FGCC Subjected to the Coupling of Penetration and Explosion. J. Mater. Civil. Eng 2021; 33(6): 04023484. https://doi.org/10.1061/(ASCE)MT.1943-5533.0003665

46. Li, Z.T., Ge Z L, Zhou Z, Mi J Y, Liu L, Shangguan J M, and Shao C F. Numerical simulation and experimental verification of heterogeneous granite impacted by abrasive water jet based on SPH-FEM coupling algorithm. Powder. Technol 2023; 416: 118233. https://doi.org/10.1016/J.POWTEC.2023.118233

47. Zhao H H, Jiang H X, Warisawa S, Li H S. Numerical study of abrasive water jet rotational slits in hard rock using a coupled SPH-FEM method. Powder Technol. 2023;426:118622, https://doi.org/doi.org/10.1016/j.powtec.2023.118622

48. Zhao H H, Jiang H X, Li H S, Zhang X D, Zhao M J. Numerical research on rock cutting by abrasive jet under confining pressure based on SPH-FEM method. Powder Technol. 2024;433: 119196. https://doi.org/doi.org/10.1016/j.powtec.2023.119196

49. Cai C, Zhang P, Xu D P, Yang X P, Zhou Y F. Composite rock-breaking of high-pressure CO2 jet & polycrystalline-diamond-compact (PDC) cutter using a coupled SPH/FEM model. Int. J. Miner. Sci. Technol. 2022;32(5):1115-24. https://doi.org/doi.org/10.1016/j.ijmst.2022.08.009

50. Xiao N, Zhou X P, Gong Q M. The modelling of rock breakage process by TBM rolling cutters using 3D FEM-SPH coupled method. Tunn. Undergr. Space Technol. 2017;61:90-103. https://doi.org/doi.org/10.1016/j.tust.2016.10.004

51. Zhu B, Jiang N, Yao Y K, Luo X D. SPH numerical simulation of SC-CO2 directional fracturing and emulsion explosives for rock breaking. Gas Sci. Eng. 2024;124:205277. https://doi.org/doi.org/10.1016/j.jgsce.2024.205277

52. Liu X H, Tang P, Li X, Tian M R. Self-rotatory performance of conical cutter interacted with rock material. Eng. Fail. Anal. 2017;80:197-209. https://doi.org/10.1016/j.engfailanal.2017.06.030

53. Guo, J.B., Zhang J H, Ma H Y, Yu H F, Wu Zh Y, Han W L, and Liu T. Dynamic Behavior of a New Type of Coral Aggregate Concrete: Experimental and Numerical Investigation. J. Mater. Civil. Eng 2023; 35(6): 04023124. https://doi.org/10.1061/JMCEE7.MTENG-14821

54. Xiao, Y.C., Gong T Y, Liu F, and Sun Y. Dynamic Mechanical Behavior and Constitutive Model of a Newly Designed Reactive Nanoinorganic Cement-Based Composite. J. Mater. Civil. Eng 2024; 36(1): 04023484. https://doi.org/10.1061/JMCEE7.MTENG-15261

55. Liu X H, Tang P, Geng Q, Wang X B. Effect of Abrasive Concentration on Impact Performance of Abrasive Water Jet Crushing Concrete. Shock Vib. 2019;2019:1-18.https://doi.org/10.1155/2019/3285150